Chinese Chemical Letters 34 (2023) 108227

Contents lists available at ScienceDirect

Chinese Chemical Letters

journal homepage: www.elsevier.com/locate/cclet

2D Cd-MOF and its mixed-matrix membranes for luminescence sensing antibiotics in various aqueous systems and visible fingerprint identifying

Kexin Ma[a], Jing Li[a], Huiyan Ma[a], Yan Yang[a], Hua Yang[a], Jing Lu[a], Yunwu Li[a,*], Jianmin Dou[a], Suna Wang[a,*], Suijun Liu[b,*]

[a] Shandong Provincial Key Laboratory of Chemical Energy Storage and Novel Cell Technology, School of Chemistry and Chemical Engineering, Liaocheng University, Liaocheng 252000, China

[b] School of Chemistry and Chemical Engineering, Jiangxi Provincial Key Laboratory of Functional Molecular Materials Chemistry, Jiangxi University of Science and Technology, Ganzhou 341000, China

ARTICLE INFO

Article history:
Received 2 January 2023
Revised 30 January 2023
Accepted 14 February 2023
Available online 16 February 2023

Keywords:
MOF luminescence sensor
Mixed-matrix membranes
Real urban river water
Antibiotic nitrofurazone
Visible fingerprint identifying

ABSTRACT

The abuse of antibiotics has brought great harm to the human living environment and health, so it is extremely significant to develop an efficient and simple method to detect trace antibiotic residues in various wastewaters. Herein, a new two-dimensional (2D) Cd-based metal–organic framework (Cd-MOF, namely **LCU-111**) and its mixed matrix membranes (MMMs) is sifted as luminescence sensors for efficient monitoring antibiotic nitrofurazone (NFZ) in various aqueous systems and applied as visible fingerprint identifying. The **LCU-111** has good selectivity, sensibility, reproducibility and anti-interference for luminescent quenching NFZ with low detection limits (LODs) of 0.4567, 0.3649 and 0.8071 ppm in aqueous solution, HEPES biological buffer, and real urban Tuhai River water, respectively. Interestingly, the luminescent test papers and MMMs allow the NFZ sensing easier and more rapid by naked eyes, only with a low LOD of 0.8117 ppm for MMMs sensor. Notably, by combining multiple experiments with density functional theory (DFT) calculations, the photo-induced electron transfer (PET) quenching mechanism is further elucidated. More importantly, potential practical applications of **LCU-111** for latent fingerprint visualization provide lifelike evidences for effective identification of individuals, which can be applied in criminal investigation.

Among varied antibiotics, nitro-containing nitrofurazone (NFZ) is widely applied to treat bacterial infection of various wounds and mucosa ulcers, or as feed additive in animal husbandry and aquaculture [1,2]. Its excessive intake and chronic accumulation *via* food chain can induce genetic defects, immunity decline, even cancer [3–5]. Due to these reasons, NFZ has been officially banned to use for humans and food related industries all over the world [6]. Therefore, it is of practical significance and urgently needed to efficiently detect NFZ in various water bodies and biological systems. Compared to complicated and high-cost technologies, luminescence detection is considered as one of the most attractive method due to its cheapness, simple, convenient, real-time and high efficient virtues [7,8], which has been widely utilized to detect organic contaminants and heavy metal pollutants [9].

Among numerous luminescent sensors, MOFs with smart structures and multiple sensing sites are notably promising candidates as high-profile luminescent probes [10,11]. Advantageously, by handpicked π-conjugated organic chromophoric modules, MOF luminescent sensors can be mediated and regulated to realize the optimal spectral regions and intensities for targeted detection. So in this study, a rigid N-rich ligand 4,5-di(1*H*-tetrazol-5-yl)-2*H*-1,2,3-triazole (H_3dttz) bearing large π-conjugated feature and multiple N-functional sites (11 N atoms in one molecule) was chosen to constructed layered 2D MOF to fulfill the NFZ detection. As is known, 2D MOFs are famous star materials by exposing more accessible surface-active sites and matching improved performance. Herein, a new 2D MOF with the formula $\{[Cd_5(dttz)_2Cl_4]\cdot 8H_2O\}_n$ (**LCU-111**) was schemed and fabricated to detect antibiotics in various aqueous systems. To facilitate detection and expand its practical application, a series of MMMs based on **LCU-111** were further prepared using a coating method [12]. The MMMs overcome the rigidity limitations of pure MOF crystals and combine the flexibil-

* Corresponding authors.
E-mail addresses: liyunwu@lcu.edu.cn (Y. Li), wangsuna@lcu.edu.cn (S. Wang), sjliu@jxust.edu.cn (S. Liu).

https://doi.org/10.1016/j.cclet.2023.108227
1001-8417/

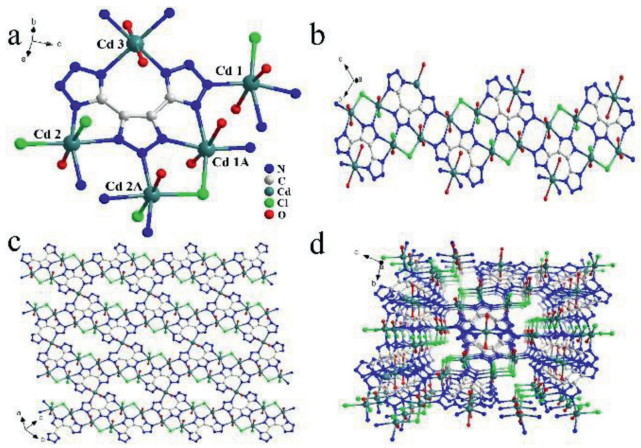

Fig. 1. (a) The coordination mode of $dttz^{3-}$ ligand. (b) The 1D chain structure. (c) The 2D layered structure. (d) The 3D stacking structure of **LCU-111**.

ity with processability of polymers to achieve a wide range of morphological features and practical sensor application devices. Besides, the homogeneous distribution of MOFs in MMMs allows for good permeability, which helps analytes to realize better contact with the MOFs compared to pure MOF sensors, resulting in improved sensing performance [13].

As expected, **LCU-111** can detect antibiotic NFZ in pure aqueous solution, simulated HEPES buffer and real river water by luminescent quenching with low LODs of 0.4567, 0.3649 and 0.8071 ppm, respectively. More importantly, **LCU-111** based MMMs can also sensing NFZ with a competitive LOD of 0.8117 ppm. A possible PET quenching mechanism is validated by UV-vis, XPS, PXRD, luminescence decay lifetime assisted with DFT calculations. Interestingly, **LCU-111** luminescent test papers provide convenience to quickly monitor NFZ by naked eyes. Due to the strong luminescence properties of **LCU-111**, a simple and visible luminescent fingerprint imaging further offers authoritative evidences to distinguish personal identity potentially toward advanced practical application [14].

The **LCU-111** isolates in triclinic crystal system with space group *P*-1 and shows a ladder-shaped 2D layered structure (Table S1 in Supporting information). The asymmetric unit of **LCU-111** consists of two and a half Cd^{2+}, one $dttz^{3-}$ ligand, two Cl^- and four coordinated H_2O molecules. Three Cd^{2+} have the same six-coordinated modes with twisted octahedron geometries but different coordinated details (Fig. 1a). All bond lengths and angles in **LCU-111** are consistent with the Cd-MOFs data reported before (Table S2 in Supporting information). Moreover, all $dttz^{3-}$ ligands possess the same eight-coordinated fashion to link five different Cd^{2+}. By chelating and bridging of $dttz^{3-}$ and Cl^-, $Cd1^{2+}$ and $Cd2^{2+}$ linked together to form a 1D wavy chain-like structure (Fig. 1b). 1D chains connected by $Cd3^{2+}$ to generate a ladder-shaped 2D layered structure (Fig. 1c). The 3D supramolecular mapping shows internal microporous structure by hydrogen bonding and π-π stacking interaction, which can allows small guest molecules access (Fig. 1d). The **LCU-111** provides affluent uncoordinated N atoms and terminal Cl^- as bifunctional sites in the pores, which can account for the luminescence specific recognition.

The solid state luminescence properties of free H_3dttz ligands and **LCU-111** were investigated at room temperature, respectively. As shown in Fig. 2a, at the excitation peak of 389 nm, **LCU-111** appears the emission peak at 466 nm. By comparison, the free H_3dttz ligands show an emission peak at 496 nm under 400 nm excitation (Fig. S1 in Supporting information). The **LCU-111** emission peak occurs an obvious blue shift *vs.* free H_3dttz ligands. The reason is that the H_3dttz ligands coordinated to Cd^{2+} (d^{10}) enhance their rigidity and led to easier transition of electrons. So the emission of **LCU-111** are caused by n-π^* or π-π^* electron transition in the ligands [9,10]. Its CIE coordinates (0.1594, 0.2243) are located in blue-green light emitting region (Fig. 2a).

LCU-111 was conducted to identify antibiotics residues in various wastewaters by luminescence sensing due to its bifunctional sites. Before practical applications in various aqueous systems, the good solution stability of **LCU-111** is checked using PXRD (Fig. S2 in Supporting information). The detailed sensing procedure of antibiotics in aqueous solution is offered in Supporting information. As shown in Fig. 2c, the luminescence intensities of **LCU-111** are different towards various antibiotics. Specifically, in NFZ solution, the **LCU-111** displays the lowest luminescence intensity, suggesting the strongest luminescent quenching. As shown in Fig. 2d, the luminescence intensity of **LCU-111** in blank aqueous solution is 4896 a.u., while it decreases to 1.5 a.u. in NFZ solution, dropping 3264 folds. In the luminescence images taken under the 365 nm UV lamp, NFZ solution has the darkest color compared to other antibiotics (Fig. 2b). This provides convenience to easily identify these antibiotics by naked eyes. The above preliminary tests indicate the **LCU-111** is an excellent NFZ luminescence quenching sensor in aqueous solution.

In order to investigate the optimal quenching effect of **LCU-111** on NFZ, luminescence titration experiments were further carried out. With the continuous addition of NFZ, the luminescence intensity decreases obviously. When adding 210 μL NFZ, the intensity drops to only 4% compared to the value of original blank sample. From Fig. 2e, the K_{sv} of **LCU-111** for NFZ is calculated as 3.96×10^4 L/mol by Stern-Volmer (S-V) equation $I_0/I = K_{sv}[M] + 1$, expressing the luminescent quenching efficiency [7]. The LOD of **LCU-111** for NFZ is 0.4567 ppm (0.1292 μmol/L) according to equation $LOD = 3\delta/k$ (Fig. 2f), which surpasses most reported MOF-based luminescence sensors (Table S3 in Supporting information) [10]. The luminescence photos of **LCU-111** in different concentrations of NFZ solutions are shown in Fig. S5 (Supporting information). As the NFZ concentration increases, the luminescence color changes gradually from bright blue-green to darker and darker. To verify the specific recognition of **LCU-111**, the anti-interference experiments of NFZ by adding other antibiotics were studied and compared. As shown in Fig. S6 (Supporting information), the strength of **LCU-111** remains low in the presence of various antibiotics. This shows that the recognition of NFZ by **LCU-111** is not affected by other antibiotics and has a good resistance to interference. Fast response is a key factor for the practical application of luminescence sensors. So a time-response experiment was also carried out, where the luminescence intensity decreases rapidly to a lowest point within 30 s after the addition of 210 μL NFZ solution, and it remains constant more than 500 s (Fig. S7 in Supporting information). In addition, **LCU-111** also has a good cycling stability and can be repeatedly reused after five cycles (Figs. S8 and S9 in Supporting information).

Overuse of antibiotics is harmful to humans, so the practical application of **LCU-111** for the detection of NFZ in real civil wastewater from the urban Tuhai River water (located in Liaocheng city, China) and HEPES simulated biological fluid are chosen to prepare the suspensions. As shown in Figs. 3a and b, Figs. S10-S12 (Supporting information), **LCU-111** can still recognize NFZ in real Tuhai River water samples and HEPES buffer. Compared with other antibiotics, the luminescence quenching effect to NFZ is still obvious. Similarly, luminescence titration experiments show that the luminescence intensity decreases continuously with the increasing of NFZ concentration (Figs. 3c and e). The K_{sv} value of **LCU-111** for NFZ is 3.38×10^4 and 1.15×10^4 L/mol in real river water and HEPES calculated by S-V equation (Figs. 3c and e) [7], respectively. The corresponding LOD of **LCU-111** for NFZ is 0.8071 and 0.3649 ppm (Figs. 3d and f) [10], respectively, which is also better than most reported MOFs sensors (Table S3). The LOD in HEPES is low-

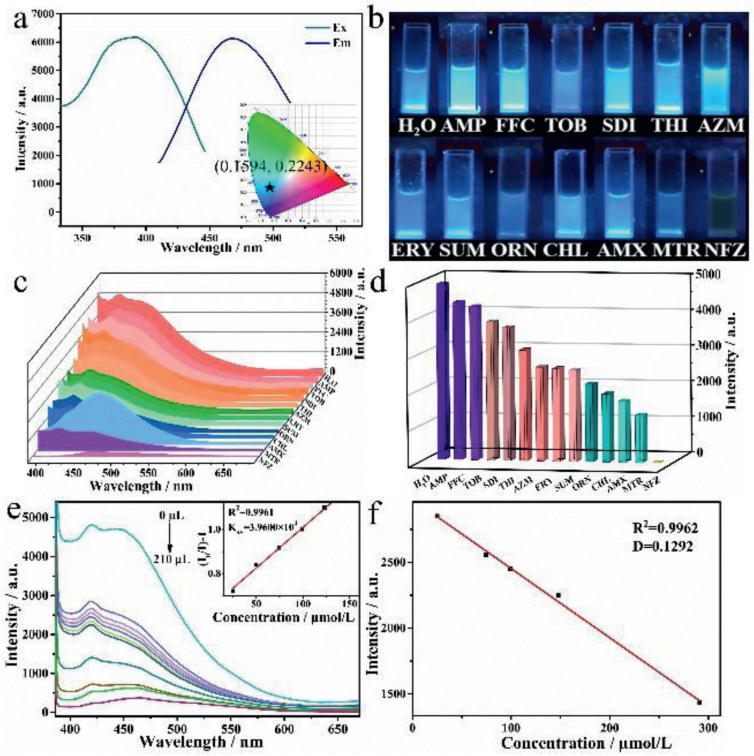

Fig. 2. (a) Solid-state excitation and emission spectrum (inset: CIE coordinate of **LCU-111**). (b) Luminescence images of **LCU-111** in different antibiotic solutions under 365 nm UV lamp. (c) The luminescence spectra and (d) intensities of **LCU-111** in various antibiotic solutions. (e) The luminescence titration curves and (f) corresponding LOD of **LCU-111** for NFZ in aqueous solution (inset: S-V plot).

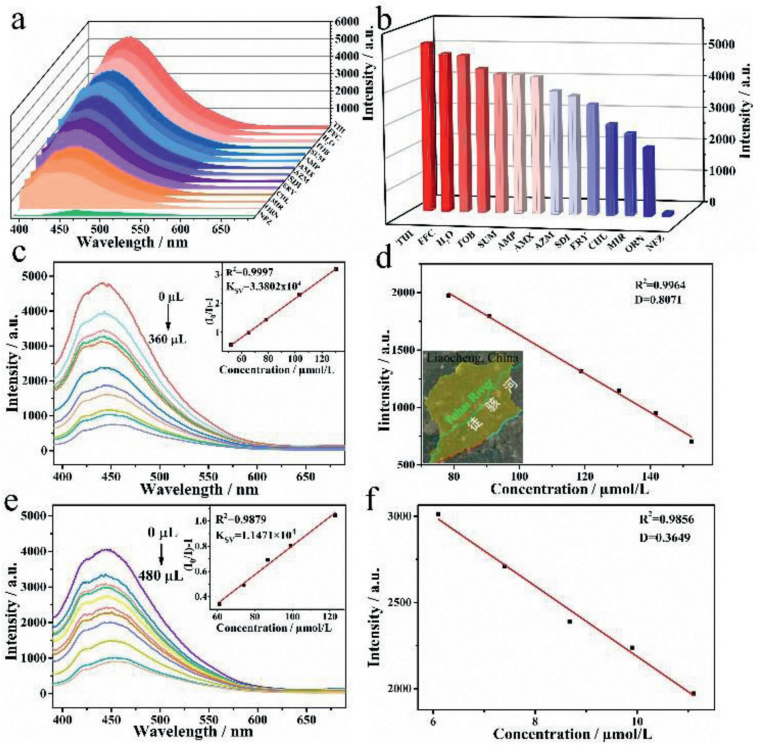

Fig. 3. (a, b) Antibiotics identification map, (c) luminescence titration experiments and (d) calculated LOD of **LCU-111** in real urban Tuhai River water (inset: the urban Tuhai River acrossing Liaocheng city, China). (e) Luminescence titration experiments and (f) calculated LOD of **LCU-111** in HEPES buffered solution.

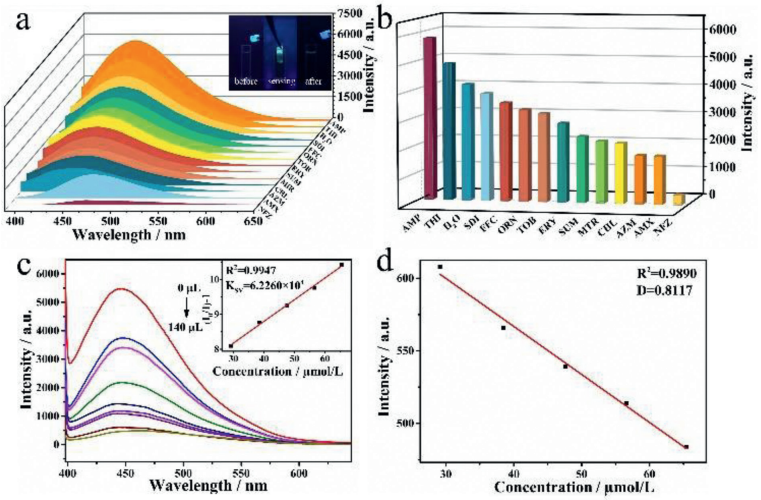

Fig. 4. (a) The luminescence spectra (inset: MMMs before and after immersion in NFZ) and (b) the luminescence intensities of **LCU-111** MMMs in various antibiotic solutions. (c) The luminescence titration experiments and (d) the calculated LOD of **LCU-111** MMMs.

est among these three aqueous systems, manifesting **LCU-111** is a good candidate as bio-sensor. The **LCU-111** still has strong anti-interference capacity for identifying NFZ against other antibiotics in real Tuhai River water (Fig. S10 in Supporting information). **LCU-111** also has a good cycling stability after five cycles (Fig. S13 in Supporting information) and fast response time (Fig. S14 in Supporting information) in real Tuhai River water. It is worth noting that the real Tuhai River water samples contain lots of complex substances and undulated pH values as a flowing river acrossing the Liaocheng city, however the **LCU-111** still has stable recognition performance in real river water, suggesting a promising application in practical wastewater detection.

Due to above excellent sensing capability of **LCU-111** toward NFZ in various aqueous systems, the luminescent MMMs were further made by drawdown coating process so as to expand its practical application [12]. Four types of MMMs are prepared (Fig. S15a in Supporting information) and the mass ratios of **LCU-111** are 0 wt%, 2 wt%, 4 wt% and 8 wt%, respectively. Taken 8 wt% MMMs as example, the PXRD spectra before and after sensing NFZ are in agreement with the crystal **LCU-111**, proving **LCU-111** based MMMs have good crystal structure stability (Figs. S17 and S18 in Supporting information). The selected 0 wt% and 8 wt% MMMs both have good ductility and plasticity (Figs. S15b-e in Supporting information). Images of 2 wt% and 4 wt% MMMs are also taken under natural light and 365 nm UV lamps (Fig. S19 in Supporting information). The SEM of 0 wt% and 8 wt% MMMs both show smooth and trim surfaces (Figs. S15f and g in Supporting information). The difference is that the 8 wt% MMMs displays obvious porous structure. According to previous reports, MMMs have better sensing performance when the MOF content is 8 wt% [12]. From Fig. S20 (Supporting information), the luminescence intensity of 8 wt% MMMs is four times higher than that of pure MMMs. Also, the luminescence sensing intensities *versus* time of four MMMs in NFZ solution were monitored, which still show 8 wt% MMMs are stable (Fig. S21 in Supporting information). So subsequent experiments were carried out using 8 wt% MMMs.

As shown in Figs. 4a and b, 8 wt% MMMs also show excellent luminescence sensing toward NFZ as expected. The luminescence intensity in blank aqueous solution is 13 times lower than in aqueous solution. As can be clearly seen from illustration of Fig. 4a, MMMs become darken in NFZ solution compared to other antibiotic solutions under UV lamp (Fig. S22 in Supporting information). Moreover, the quenching titration experiment is shown that the luminescence intensity decreases gradually with the addition of NFZ solution (Fig. 4c). After the addition of 140 μL NFZ, the luminescence intensity reduces to 8% *versus* the original value. The calculated K_{sv} of **LCU-111** MMMs for NFZ is as high as 6.23×10^4 L/mol [7], and the corresponding LOD is 0.8117 ppm (Figs. 4c and d), also lower than most reported MOFs sensors (Table S3) [10]. Competition experiments show that **LCU-111** MMMs still have strong anti-interference ability for quenching NFZ in mixture with other antibiotics (Fig. S23 in Supporting information). The **LCU-111** MMMs also have fast response time for only 20 s, and then remain stable for more than 300 s (Fig. S24 in Supporting information). These results indicate that **LCU-111** MMMs have efficient and stable sensing performance of NFZ in aqueous solution, illustrating its well practical application value.

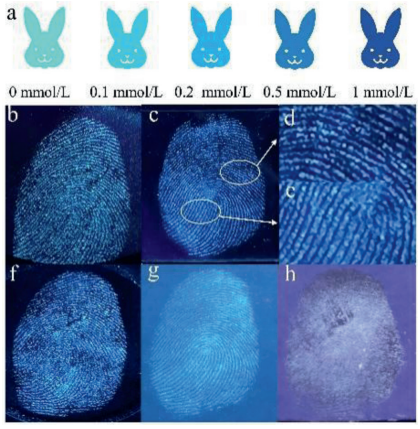

Fig. 5. (a) Luminescent test papers of **LCU-111** for NFZ under UV lamp. Luminescence fingerprint photographs of **LCU-111** on (b) steel, (c) glass, (f) plastic, (g) print paper, and (h) invoice paper. (d, e) The enlarged bifurcation and whorls of the fingerprints on glass.

To facilitate the monitoring more simply in real-world application, luminescent test papers of **LCU-111** were made to quickly detect NFZ (Fig. 5a) and other antibiotics (Fig. S25 in Supporting information). When gradually dropped NFZ solution onto the test papers, their colors are turning ever more deepened under UV light, that is, from light blue to dark blue (Fig. 5a). Moreover, fingerprint is one of the most concerned material evidences to identity recognition due to its uniqueness of everyone and unchanged throughout life. So based on the strong luminescence properties of **LCU-111**, a simple and visible luminescent fingerprint identification was

proposed. Fingerprints were printed on smooth surfaces of different substrates such as plastic, steel, glass and various papers [14]. The fingerprints are invisible in sunlight, but vivid fingerprint patterns on a variety of substrates appear under 365 nm UV light (Figs. 5b-h). Interestingly, the fingerprint patterns are clearer on steel and glass than on plastic, print paper and invoice paper, respectively, indicating that the **LCU-111** particles bind more strongly on steel and glass surfaces than on others. Furthermore, three-level detailed fingerprint features can be clearly observed by naked eyes, such as patterns of whorls and loops (level-one), ridge ending and bifurcation (level-two), and even scars (level-three) (Figs. 5b-f). These unique characteristic informations provide authoritative evidences to distinguish personal identity toward advanced practical application of **LCU-111**.

The quenching mechanism of **LCU-111** for NFZ was further verified by XPS, PXRD, UV-vis, luminescence decay lifetime and DFT calculations. Firstly, the PXRD after 3 days immersed in NFZ solution is the same as original crystal **LCU-111**, indicating the framework structure of **LCU-111** remains intact after sensing (Fig. S2), ruling out the structural collapse led to luminescent quenching. Secondly, the UV-vis absorption spectrum of NFZ-treated **LCU-111** does no overlap with the luminescence excitation spectrum ($\lambda_{ex} = 389$ nm) of the original **LCU-111** (Fig. S26 in Supporting information), suggesting that the competitive energy absorption of the NFZ and **LCU-111** is not responsible for the luminescence quenching. Thirdly, the XPS show that the binding energies of Cd 3d, O 1s, N 1s and Cl 2p all arise blue-shift from 406.1, 532.9, 400.6, 198.8 eV to 406, 532.8, 400.3, 198.7 eV, respectively, indicating the occurrence of interaction between NFZ and the **LCU-111** skeleton (Figs. S27 and S29a-d in Supporting information). Lastly, the interaction is further verified by the luminescence decay lifetime results (Fig. S28 in Supporting information), which reduces *ca.* 12% for NFZ-treated **LCU-111** (3.6515 μs) *vs.* the original lifetime (4.1278 μs).

Based on the above series of experiments, the luminescence quenching of **LCU-111** toward NFZ may possibly be attributed to the PET mechanism, where electron transfer can cause weak interaction, and further result in luminescence quenching. A typical PET system is composed of a receptor, a spacer, and a fluorophore donor. In a PET luminescent molecular probe, the conversion between the recognition group and fluorophore is accomplished by light-induced electron transfer. Generally, the PET process is triggered by the energy gap of the LUMO between the photo-excitation donor and acceptor [15–18]. Since the luminescence of **LCU-111** is mainly derived from the H_3dttz ligands with rich delocalized electrons, and the NFZ has a strong electron-absorbing group (-NO_2), the PET process can occur from H_3dttz to the LUMO of NFZ [18]. To further verify this conjecture, DFT calculations were performed using the B3LYP/6-31G* motif [15–18]. As shown in Fig. S29e (Supporting information), the LUMO energy level of H_3dttz (-2.00 eV) is higher than that of NFZ (-3.02 eV), so the PET execute electron transfer from H_3dttz to NFZ, and thus induce the best quenching performance. Moreover, in contrast, only the HOMO and LUMO energy of the NFZ among all sensing antibiotics both locate between the HOMO and LUMO energy of H_3dttz (Fig. S30 in Supporting information), which further validates more easily recognized of NFZ. Therefore, the luminescence quenching mechanism of **LCU-111** toward NFZ can be attributed to the PET mechanism.

In conclusion, a new 2D Cd-MOF **LCU-111** has been picked as a luminescent quenching sensor for efficient detecting antibiotic NFZ in aqueous solution, HEPES biological buffer, and real urban river water with low LODs of 0.4567, 0.3649 and 0.8071 ppm, respectively. The sensor is gifted with good selectivity, sensitivity, stability and anti-interference ability in above various aqueous systems due to more exposed functional sites of 2D material. Moreover, the luminescent test papers of **LCU-111** realize quickly, real-time and visual monitor NFZ by naked eyes. Notably, **LCU-111** based MMMs further provide flexible practical applications for quenching NFZ also with a low LOD of 0.8117 ppm. A reasonable PET quenching mechanism is demonstrated by experiment metrics plus DFT calculations. Latent fingerprint visualization of **LCU-111** can support the security sectors to precisely identify criminals.

Declaration of competing interest

The authors declare that they have no known competing financial interests or personal relationships that could have appeared to influence the work reported in this paper.

Acknowledgments

This work was financially supported by the National Natural Science Foundation of China (Nos. 21771095 and 22061019), the Natural Science Foundation of Shandong Province (Nos. ZR2021MB114 and ZR2021MB073), and the Youth Innovation Team of Shandong Colleges and Universities (No. 2019KJC027).

Supplementary materials

Supplementary material associated with this article can be found, in the online version, at doi:10.1016/j.cclet.2023.108227.

References

[1] Y.Z. Tang, H.L. Huang, W.J. Xue, et al., Chem. Eng. J. 384 (2020) 123382.
[2] H.K. Li, H.L. Ye, X.X. Zhao, et al., Chin. Chem. Lett. 32 (2021) 2851–2855.
[3] Q.Q. Chu, B. Zhang, H.F. Zhou, et al., Inorg. Chem. 59 (2020) 2853–2860.
[4] S.L. Hou, J. Dong, X.L. Jiang, et al., Anal. Chem. 90 (2018) 1516–1519.
[5] H.T. Bai, H.X. Yuan, C.Y. Nie, et al., Angew. Chem. Int. Ed. 127 (2015) 13406–13411.
[6] L. Ding, Y.Y. Zhao, H.H. Li, et al., J. Hazard. Mater. 416 (2021) 125759.
[7] Z.Z. Liang, H.B. Guo, H.T. Lei, et al., Chin. Chem. Lett. 33 (2022) 3999–4002.
[8] X.P. Quan, B. Yan, ACS Appl. Mater. Interfaces 14 (2022) 49072–49081.
[9] Z.J. Ke, K.X. Chen, Z.Z. Li, et al., Chin. Chem. Lett. 32 (2021) 3109–3112.
[10] J.J. Hou, P. Jia, K.R. Yang, et al., ACS Appl. Mater. Interfaces 14 (2022) 13848–13857.
[11] H.K. Li, Z.Y. Han, Q.Q. Zhu, et al., Chin. Chem. Lett. 32 (2021) 2865–2868.
[12] L.L. Wang, P.L. Zheng, W.L. Zhang, et al., Mater. Today Commun. 16 (2018) 258–263.
[13] H.H. Yu, Q. Liu, M.Y. Fan, et al., Dyes Pigm. 197 (2022) 109812.
[14] S.J. Zhang, R.H. Liu, Q.L. Cui, et al., ACS Appl. Mater. Interfaces 9 (2017) 44134–44145.
[15] N. Seal, M. Singh, S. Das, et al., Mater. Chem. Front. 5 (2021) 979–994.
[16] Y. Li, B.L. Chai, H. Xu, et al., Inorg. Chem. Front. 9 (2022) 1504–1513.
[17] W.P. Lustig, S. Mukherjee, N.D. Rudd, et al., Chem. Soc. Rev. 46 (2017) 3242–3285.
[18] H. Zheng, Y.K. Deng, M.Y. Ye, et al., Inorg. Chem. 59 (2020) 12404–12409.